Electronic Supplementary Information of:

Vibrational Circular Dichroism Under the Quantum Magnifying Glass: From the Electronic Flow to the Spectroscopic Observable

Marco Fusè,[a] Franco Egidi,*[a] and Julien Bloino*[a]

Contents

[a] *Scuola Normale Superiore, Piazza dei Cavalieri 7,56126 Pisa, Italia; E-mail: franco.egidi@sns.it; julien.bloino@sns.it*

1 Equations for the atomic tensors

Here we report the full equations used to calculate the nuclear and electronic parts of the atomic polar and axial tensors in terms of the vibrational transition current density (VTCD). Both quantities can be expressed in either Cartesian coordinates or using mass-weighted normal modes. In the manuscript we chose to employ the latter representation because it can be readily used to write equations for the infra red (IR) or vibrational circular dichroism (VCD) intensity.

The relationships between Cartesian $\mathbf{R}_\alpha$ and normal mode Q_i coordinates, as well as the corresponding momenta $\mathbf{p}_\alpha$ and P_i, can be written as:

$$\mathbf{R}_\alpha - \mathbf{R}^0_\alpha = \Delta\mathbf{R}_\alpha = M_\alpha^{-1/2} \sum_i \mathbf{L}_{\alpha i} Q_i \quad ; \quad \mathbf{p}_\alpha = M_\alpha^{1/2} \sum_i \mathbf{L}_{\alpha i} P_i$$

Where the subscript α runs over all atoms, M_α are the atomic masses, $\vec{R}^0$ are the nuclear coordinates at the equilibrium geometry, and $\mathbf{L}$ is a unitary matrix that diagonalizes the mass-weighted molecular Hessian. In our notation $\mathbf{L}_{\alpha i}$ is a three-component vector whose components are related to the Cartesian coordinates of atom α. Note that the matrix $\mathbf{L}$ is more commonly expressed using a notation where the first index spans over all atomic coordinates rather than all atoms, however the vector notation is helpful when writing the components of the atomic axial tensor.

The nuclear part of the atomic polar tensor for normal mode i is computed from the total nuclear electric dipole moment:

$$\mathbf{U}_i^{\text{nuc}} = \frac{\partial}{\partial Q_i} \sum_\alpha eZ_\alpha \mathbf{R}_\alpha = \frac{\partial}{\partial Q_i} \sum_\alpha eZ_\alpha (\mathbf{R}^0_\alpha + \Delta\mathbf{R}_\alpha) = \sum_\alpha eZ_\alpha M_\alpha^{1/2} \mathbf{L}_{\alpha i}$$

The nuclear part of the atomic axial tensor is instead calculated from the nuclear magnetic dipole moment:

$$\mathbf{M}_i^{\text{nuc}} = \frac{\mathrm{i}}{2\hbar} \left(\frac{\partial \mathbf{m}^{\text{nuc}}}{\partial P_i} \right)_{Q=0} = \frac{\mathrm{i}}{2\hbar} \frac{\partial}{\partial P_i} \sum_\alpha \frac{eZ_\alpha}{2M_\alpha c} \Delta\mathbf{R}_\alpha \times \mathbf{p}_\alpha = \frac{\mathrm{i}}{2\hbar} \sum_\alpha \frac{eZ_\alpha}{2c} M_\alpha^{-1/2} \mathbf{R}^0_\alpha \times \mathbf{L}_{\alpha a}$$

2 Vector field representation

As mentioned in section 3.2 of the main text, the simplest method for graphically depicting vector fields is the so-called hedgehog representation, in which vectors are depicted as glyphs, such as lines or arrows. Since a plain hedgehog representation in which every vector of the data set is explicitly depicted is unfeasible, some sort of simplification is required. For this reason, we tried the projection of the 3D data-set onto specific planes that,for smaller systems, can be a solution, see for instance the figures 1.ESIa and 1.ESIb. A first limitation in this kind of approach is that it is not feasible for bigger systems, indeed the presence of different atoms along a projection coordinate would risk of producing artifacts or tangled representations. The second limitation is intrinsic of the representation technique, in glyph based visualization for vector dataset the representation cannot be *dense* as in the case of scalar field color mapping,producing discrete images as in the nature of the data-set. The interpolation process is left to the human perception, that in cases where the direction of the neighbors vectors varies greatly can become extremely hard up to be extremely confusing when hundreds of vectors are present.[1] In order to overcome this last limitation, we tried to interpolate the vector field with streamlines. The so-called *stream objects*, such as streamlines, are another widespread class of visual representations for visualizing flow fields.[1] Stream objects are generated on the base of the path covered by a set of imaginary particles (seeds) when inserted in the (steady or unsteady) vector field. The main difficulty when adopting these representations is the choice of the number and position of the seeding particles. A review of this class of techniques is presented in McLoughlin et al. in Ref. 2. In figures 1.ESIc and 1.ESId a representation with streamlines obtained with the builtin function in matplotlib `streamplot` is reported.[3] The thickness and color are function of the magnitude of the vector field, while the stream direction is pointed out by an arrow at the mid point of the streamline. In this representation, the flows are more clear and easy to follow, however regions of the space where the field is actually low appear as magnified. In figures 1.ESIe and 1.ESIf another type streamlines representation is presented. In this second type,[4] the streamlines are more dense and their transparency is function of the magnitude of the field, the field magnitude is also depicted by a color-map in the background, whereas the direction of the stream is left to an animation of the streamlines.

Moving to a 3D representation it is possible overcome the problems of the overlays between the different atoms in the systems, allowing a better representation of the VTCD around the molecules. Approaching a 3D space a simplification of the data-set is mandatory. Starting with an hedgehog representation, the simpler possible approach is to divide the data-set in regions containing elements having a strong similarity between them and a weak similarity with the elements belonging to the other regions, by performing a cluster analysis on the elementary vectors.[5] Once a simplified vector field is derived by means of a clustering procedures, it can then be visualized using a glyphs. In figure 2.ESIa the VTCD associated to the 4^{th} normal modes of the (2*S*,3*S*)-oxirane-d_2 is represented with the hedgehog representation after the clustering of the vector field using the agglomerative hierarchical clustering algorithm recently implemented in CAFFEINE,[6–8] whereas in figure 2.ESIb a 3D streamline representation of the same vector field is reported. The main advantages of the 3D representation are discussed in the main text (see section 3.2), here we focus our attention to the main differences between the two type of chosen representations. Although in figure 2.ESIa the direction at each point of the represented field is easier to get, the patterns and the overall direction of the flows is better depicted in figure 2.ESIb allowing a better and more immediate comprehension of the system.

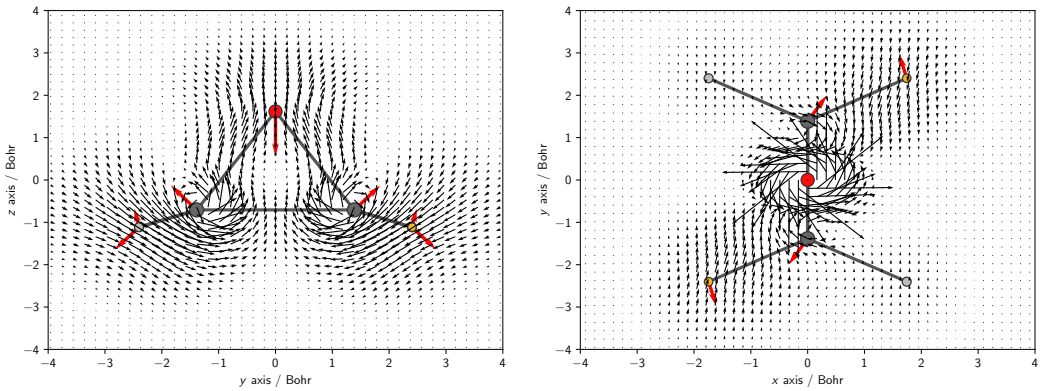

(a) *yz* plane

(b) *xy* plane

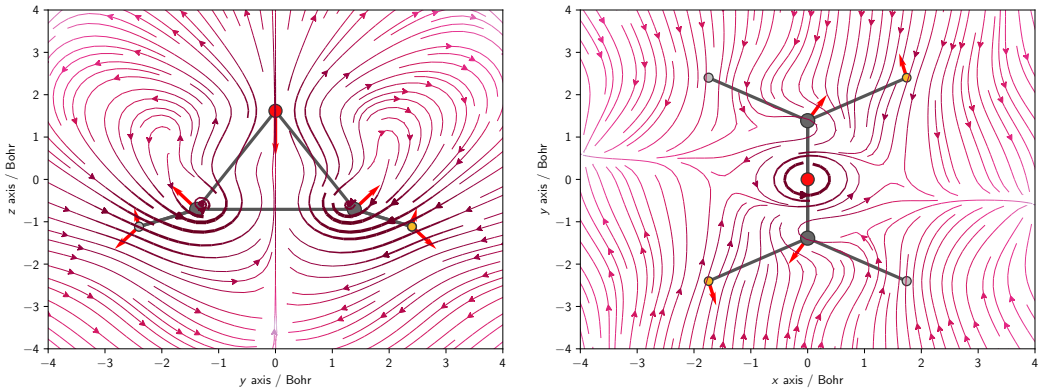

(c) *yz* plane

(d) *xy* plane

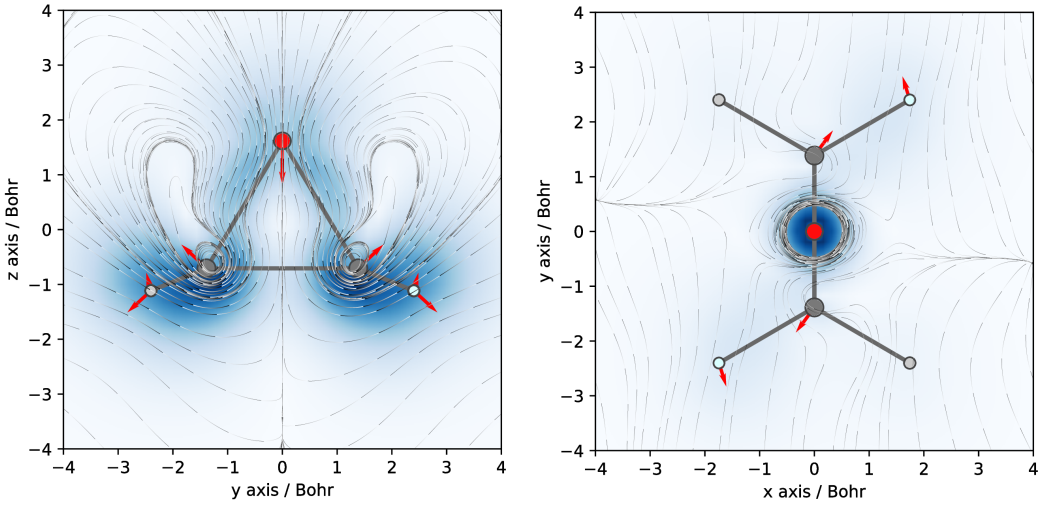

(e) *yz* plane

(f) *xy* plane

Fig. 1.ESI Different types of 2D representation of the VTCD vector fields. In each case the the VTCD has been summed over the grid points along on of the axis and projected on the orthogonal plane. Both $\mathbf{U}_i$ and $\mathbf{M}_i$ lie along the z axis. 1.ESIa and 1.ESIb the VF has been represented with quiver representation, each point point of the discrete grid has been represented as arrow which length is proportional to the intensity of the field. 1.ESIa and 1.ESIb the VF has been represented as stream lines with the built-in functionality of the matplotlib packages, the thickness and color map of the stream are function of the field intesity.[3] 1.ESIa and 1.ESIb the VF has been represented with different type of stream line shading as a function of the field intensity,[4] moreover the background has been as well colored as function of the VTCD in that point.

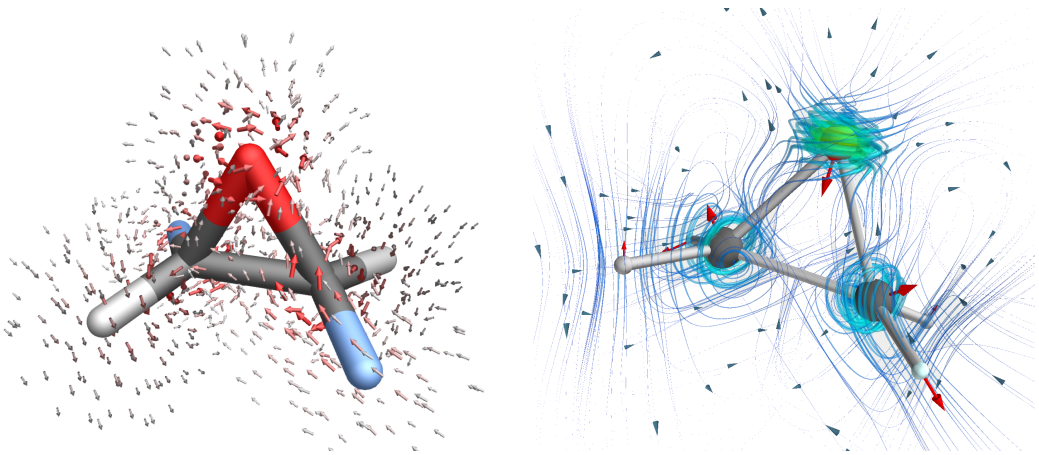

(a) Hedgehog representation

(b) Streamlines representation

Fig. 2.ESI 3D representation of VTCD vector field for the 1_4 fundamental band of (2*S*,3*S*)-oxirane-d_2. On the left (2.ESIa) hedgehog representation, 10000 representative glyphs obtained with the agglomerative hierarchical clustering algorithm implemented in caffeine,[7] and then filtered by absolute magnitude. The arrows color and size are functions of the related vector's magnitude. On the right (2.ESIb) streamlines representations of the same fields, by means of a streamline object.[9] The red arrows depict the charge-weighted nuclear displacement vector for the normal mode.

3 1,3-difluoroallene: excited states number

In the case of the 1,3-difluoroallene that was used as pilot application to include anharmonic corrections in the VTCD maps, we chose to stop the sum over state at the 100^{th} instead of 300^{th} as in the harmonic cases. This truncation of the sum-over-state was mainly due to the computational cost, especially in time, required by this approach (figure 3.ESI). However, as shown in figure 4.ESI, the main features of the VTCD plot are already present when 100^{th} excited state are included. In particular, the flux along the two double bonds (see figure 4.ESIa and 4.ESIc) and the counterclockwise rotation of charge around the two Florine atoms (figure 4.ESIb and 4.ESId) are already well depicted.

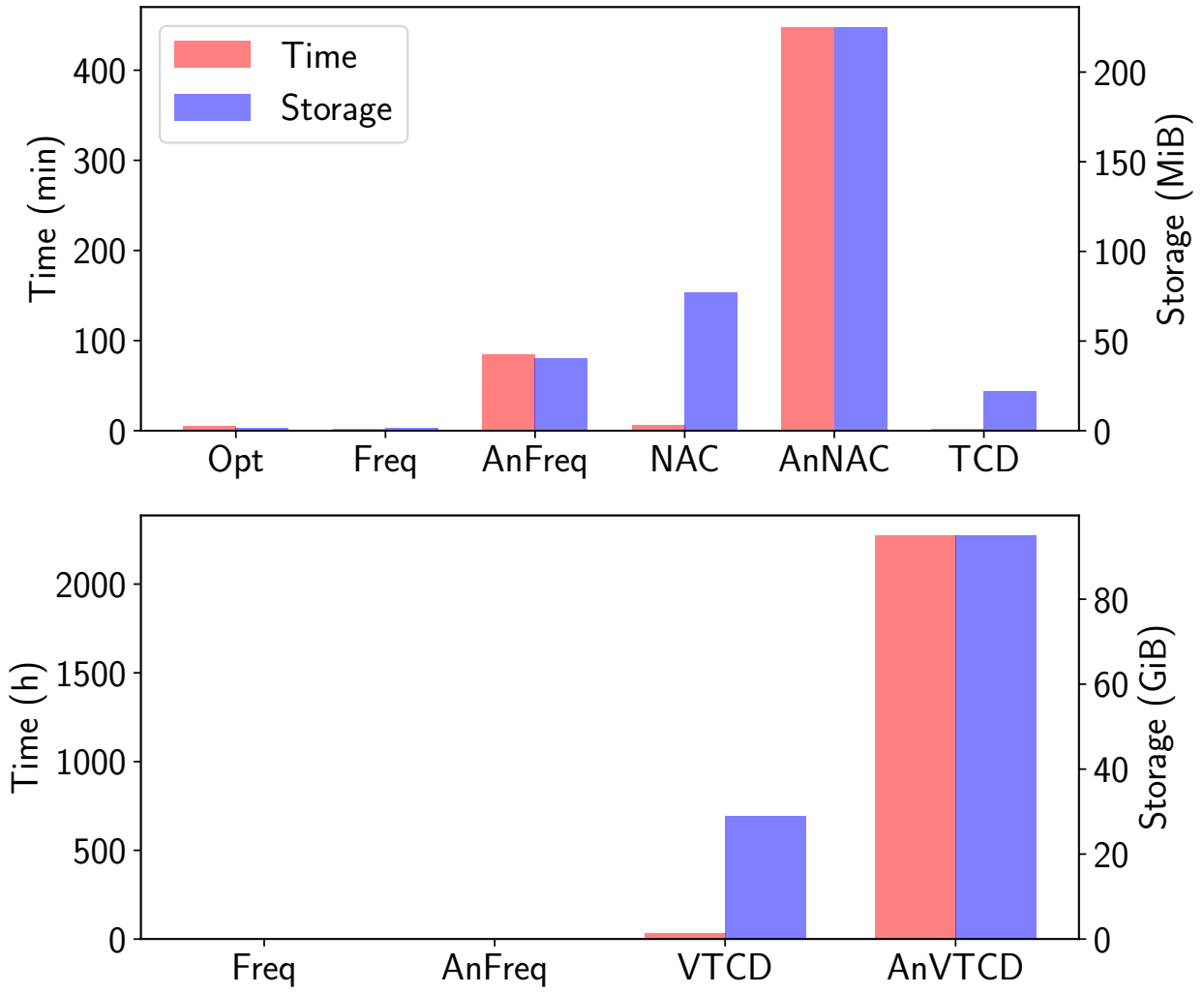

Fig. 3.ESI Top panel, computational costs of the single calculations required in for harmonic and anharmonic VTCD calculation. Bottom panel, comparison between the computation cost in time and storage space required of an harmonic frequency calulatin, an anharmonic frequency calculation, an harmonic VTCD calculation and an anharmonic VTCD calculation. The time data refer to the CPU time for calculations run on 16 cores CPU @3.30GHz with 120GB of RAM. Grind cubes of $81\times81\times81$ have been computed in the TCD calculations.

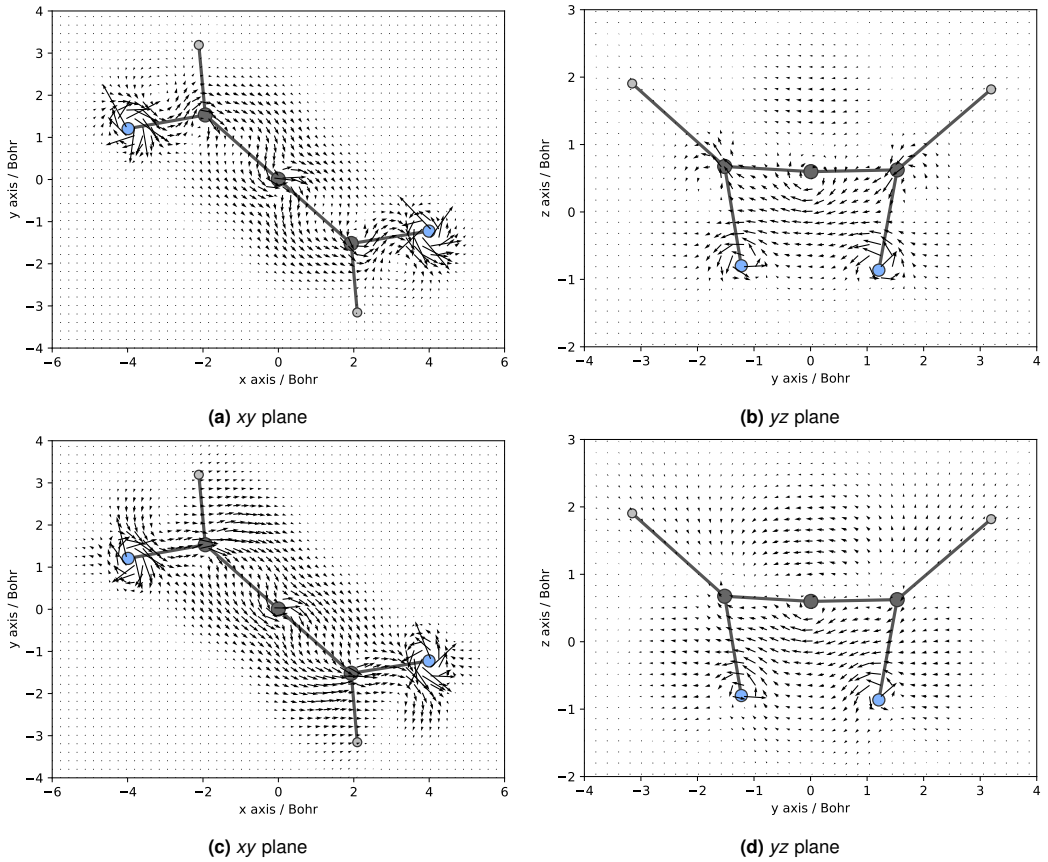

(a) *xy* plane **(b)** *yz* plane

(c) *xy* plane **(d)** *yz* plane

Fig. 4.ESI Top panels (4.ESIa and 4.ESIb): harmonic VTCD vector field with the sum over states stopped at the 100$^{\text{th}}$ for the 1_9 fundamental band of 1,3-difluoroallene. The reference system has been oriented so that *y* axis matches the $\mathbf{U}_i$ direction. In the bottom panels (4.ESIc and 4.ESId) the sum over states has been extended up to the 300$^{\text{th}}$ excited state.

4 1,3-difluoroallene: nuclear displacements

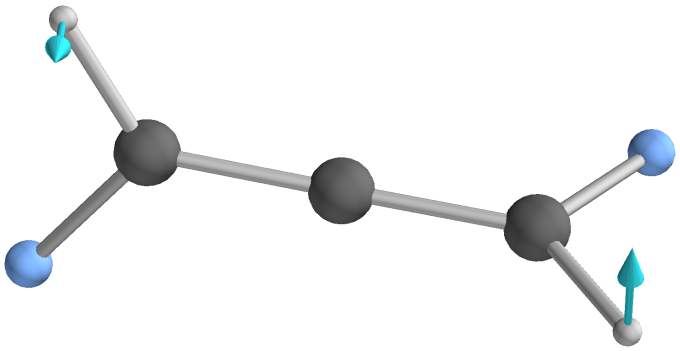

(a) 1_4

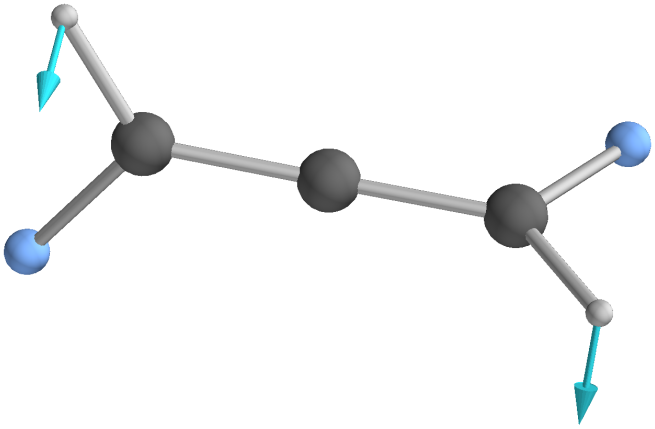

(b) 1_5

Fig. 5.ESI Nuclear displacements associated with the 1_4 and the 1_5 fundamental band of the 1,3-difluoroallene.

5 1,3-difluoroallene: NAC derivatives

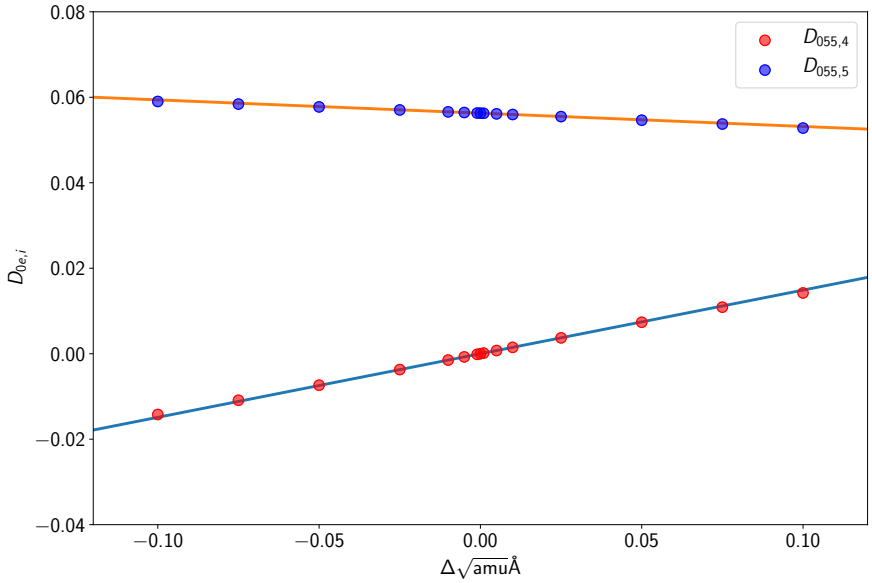

Fig. 6.ESI Non-adiabatic couplings associated with two representative vibrations, 1_4 and 1_5, evaluated at different displacements along the normal coordinates. The chosen step of 0.01 $\sqrt{\text{amu}}$Å lies in the linearity range of the functions.

6 1,3-difluoroallene: Anharmonic Transition Moments

In the following tables the anharmonic contributions at the dipole transition moments computed making use of the generalized VPT2 (GVPT2) scheme are reported.

Table 1.ESI 1_9 Fundamental band: Anharmonic Transition Moments

Electric dipole			
Term	x	y	z
Harmonic	0.72354×10^{-1}	-0.11380	0.95220×10^{-9}
Electrical	0.36559×10^{-3}	-0.70391×10^{-4}	-0.44334×10^{-18}
Mixed	-0.11096×10^{-3}	0.50392×10^{-3}	0.38195×10^{-11}
Mechanical	-0.45697×10^{-3}	0.14605×10^{-3}	-0.95251×10^{-11}
Total	0.72152×10^{-1}	-0.11322	0.94650×10^{-9}
Magnetic dipole			
Term	x	y	z
Harmonic	-0.12686×10^{1}	-0.20255	-0.60803×10^{-8}
Electrical	-0.24377×10^{-2}	-0.41333×10^{-2}	-0.20283×10^{-16}
Mixed	0.21220×10^{-2}	-0.92486×10^{-2}	-0.10343×10^{-8}
Mechanical	0.43269×10^{-1}	0.11142×10^{-1}	0.34688×10^{-9}
Total	-0.12257×10^{1}	-0.20479	-0.67677×10^{-8}

Table 2.ESI $1_5 1_4$ Combination band: Anharmonic Transition Moments

Electric dipole			
Term	x	y	z
Electrical	-0.24904×10^{-3}	-0.16445×10^{-2}	-0.63435×10^{-11}
Mechanical	-0.97115×10^{-2}	0.14325×10^{-1}	-0.14850×10^{-9}
Total	-0.99606×10^{-2}	0.12680×10^{-1}	-0.15484×10^{-9}
Magnetic dipole			
Term	x	y	z
Electrical	-0.31207×10^{-1}	0.18393×10^{-1}	-0.11491×10^{-8}
Mechanical	0.18632	0.24136×10^{-1}	0.11999×10^{-8}
Total	0.15511	0.42529×10^{-1}	0.50894×10^{-10}

7 1,3-difluoroallene: Anharmonic Spectra

Table 3.ESI Theoretical anharmonic (anharm) and harmonic(harm) Transition energies (E) in cm^{-1}, Dipole strengths (DS) in 10^{-40} esu^2cm^2 and Rotational strengths (RS) in 10^{-44} esu^2cm^2 of 1,3-difluoroallene in the $500-1400$ cm^{-1} range.

Transition	E(harm)	E(anharm)	DS(harm)	DS(anharm)	RS(harm)	RS(anharm)
$1_3 1_1$	520.10	511.69		0.06		0.04
1_4	546.21	533.56	58.57	56.32	−14.39	−14.38
$1_3 1_2$	568.82	558.67		0.42		0.03
1_5	665.32	654.52	234.07	222.71	2.46	5.91
$1_4 1_1$	688.83	672.56		1.34		−0.45
$1_4 1_2$	737.55	719.97		8.81		−2.69
2_3	754.96	743.82		0.57		−0.16
$1_5 1_1$	807.94	793.72		2.57		0.51
1_6	851.91	832.72	17.65	18.47	4.78	3.11
$1_5 1_2$	856.66	836.30		2.36		−0.55
1_7	906.49	885.63	36.43	38.43	−2.03	−2.20
$1_4 1_3$	923.68	905.44		0.34		−0.50
$1_6 1_1$	994.54	972.21		0.09		−0.07
1_8	1009.91	997.23	215.74	220.98	−102.04	−103.33
$1_5 1_3$	1042.79	1026.82		0.41		0.15
$1_6 1_2$	1043.26	1018.09		1.68		−0.70
$1_7 1_1$	1049.11	1024.68		0.01		0.01
2_4	1092.41	1061.12		0.38		−0.31
$1_7 1_2$	1097.83	1071.73		11.96		2.87
1_9	1124.21	1097.63	1174.91	1164.52	177.78	168.75
$1_8 1_1$	1152.54	1136.89		0.00		−0.02
$1_8 1_2$	1201.25	1185.63		1.54		1.12
$1_5 1_4$	1211.52	1188.75		16.80		2.60
$1_6 1_3$	1229.39	1204.78		1.65		0.48
1_{10}	1247.85	1222.28	85.24	79.76	−73.44	−68.18
$1_9 1_1$	1266.84	1237.12		1.48		−0.52
$1_7 1_3$	1283.97	1257.65		1.40		−1.58
$1_9 1_2$	1315.56	1283.22		0.25		−0.27
2_5	1330.63	1308.38		0.00		0.01
1_{11}	1358.75	1330.66	73.38	65.47	−3.35	−3.57
$1_8 1_3$	1387.39	1370.35		0.04		0.08
$1_6 1_4$	1398.12	1365.57		1.28		0.35
$1_7 1_4$	1452.69	1417.68		0.00		0.02
$1_9 1_3$	1501.69	1468.62		0.30		−0.37
$1_6 1_5$	1517.23	1486.10		0.29		−0.17
$1_8 1_4$	1556.12	1532.77		0.14		0.13
$1_7 1_5$	1571.80	1539.41		0.57		−0.39
$1_8 1_5$	1675.23	1650.35		2.57		0.15
$1_7 1_6$	1758.40	1714.74		12.75		−0.42
$1_8 1_6$	1861.83	1828.58		0.54		−0.07
$1_8 1_7$	1916.40	1881.52		0.12		0.09

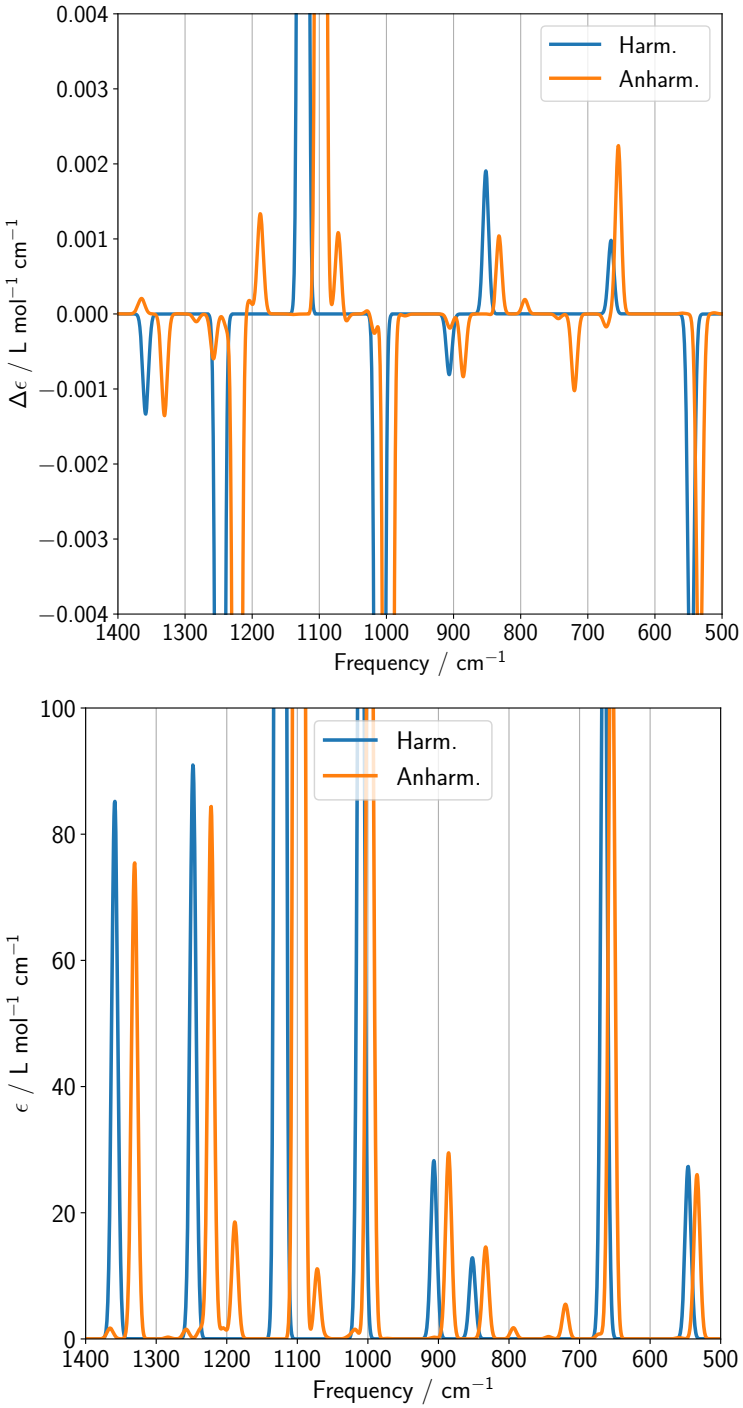

Fig. 7.ESI Theoretical anharmonic and harmonic IR (bottom) and VCD spectra (top) of 1,3-difluoroallene in the $500-1400\ cm^{-1}$ range, the y-ranges have been chosen to magnify the combination and overtone bands. The theoretical line-shapes have been convoluted by means of Lorentzian distribution functions with half-widths at half-maximum of $5\ cm^{-1}$

8 Substituted Alanine: Dipole Transition Moments

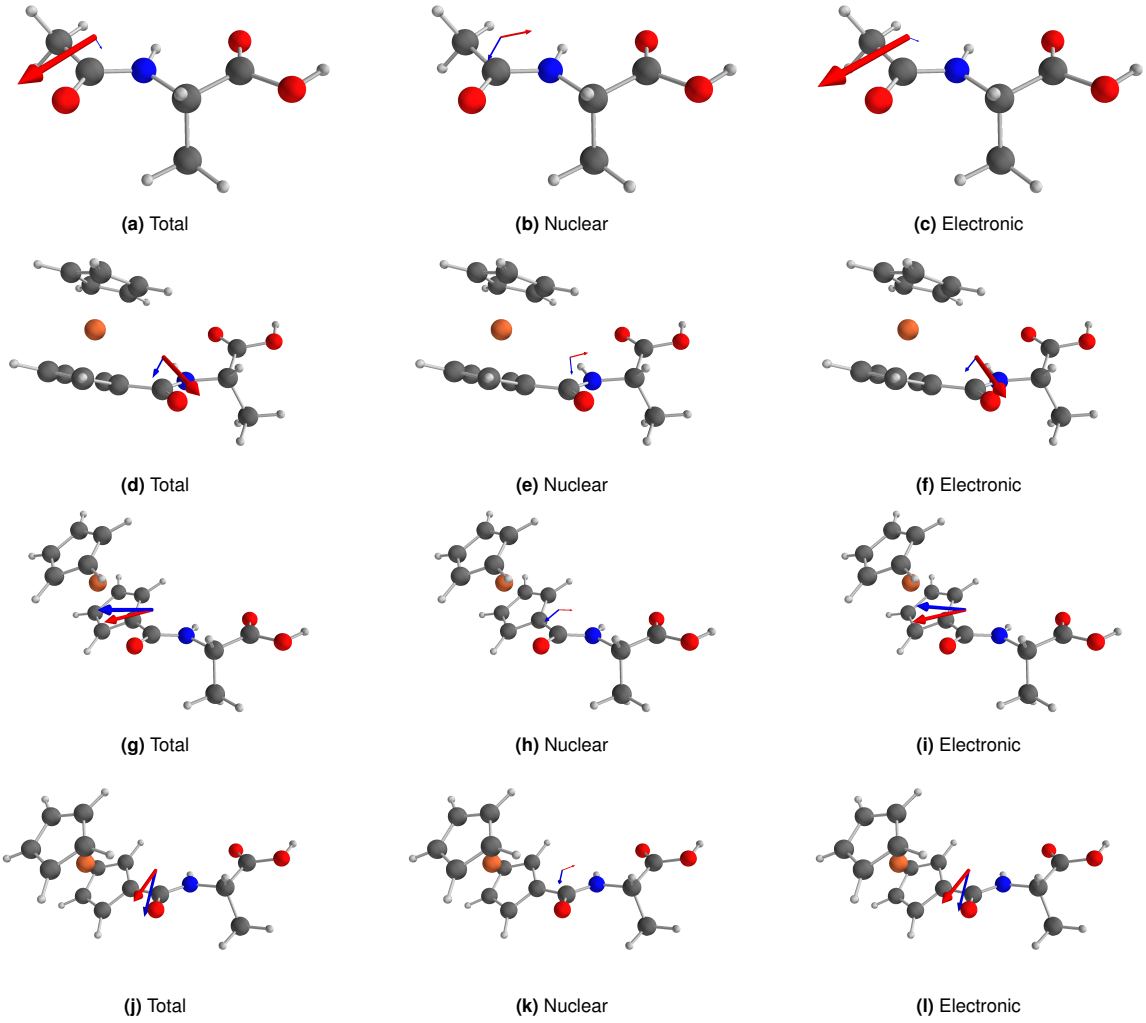

(a) Total **(b)** Nuclear **(c)** Electronic

(d) Total **(e)** Nuclear **(f)** Electronic

(g) Total **(h)** Nuclear **(i)** Electronic

(j) Total **(k)** Nuclear **(l)** Electronic

Fig. 8.ESI 3D representations of the atomic polar ($\mathbf{U}$) in red and axial ($\mathbf{M}$) tensors in blue for the amide I vibration of Ala, FeII-Ala, FeIII-Ala, at their respective minimum energy geometry, and FeII-Ala at the geometry of FeIII-Ala.

Table 4.ESI Atomic polar ($\mathbf{U}$) and axial ($\mathbf{M}$) tensors for the amide I vibration of Ala, FeII-Ala, FeIII-Ala, at their respective minimum energy geometry, and FeII-Ala at the geometry of FeIII-Ala, and the angle between them.

AcAla							
	$\mathbf{U}_i$			$\mathbf{M}_i$			Angle
	x	y	z	x	y	z	
TOT:	2.67256×10^{1}	−5.36201	-5.39575×10^{-1}	1.05123	2.92833	−2.02653	82.34
NUC:	−1.03117	2.33874	1.06801	1.79639	-1.86898×10^{-1}	−1.53656	126.75
EL :	2.77568×10^{1}	−7.70075	−1.60758	-7.44131×10^{-1}	3.11624	-4.89728×10^{-1}	117.98
FeII-Ala							
	$\mathbf{U}_i$			$\mathbf{M}_i$			Angle
	x	y	z	x	y	z	
TOT:	2.68537×10^{1}	1.68649	−6.25439	5.61428	−6.05430	−5.89854	50.73
NUC:	-1.57525×10^{-1}	2.41084	4.30966×10^{-1}	9.28241×10^{-1}	-4.86491×10^{-2}	−1.95978	102.02
EL :	2.70112×10^{1}	-7.24350×10^{-1}	−6.68536	4.68588	−6.00556	−3.93956	48.79
FeIII-Ala							
	$\mathbf{U}_i$			$\mathbf{M}_i$			Angle
	x	y	z	x	y	z	
TOT:	2.17791×10^{1}	−9.14203	1.47355×10^{-2}	2.37354×10^{1}	-1.08747×10^{1}	5.35301	11.70
NUC:	-7.81768×10^{-1}	1.77512	1.16654×10^{-1}	3.36977	-2.50945×10^{-1}	-6.17863×10^{-1}	118.18
EL :	2.25609×10^{1}	-1.09171×10^{1}	-1.01918×10^{-1}	2.03657×10^{1}	-1.06237×10^{1}	5.97094	14.90
FeII-Ala@FeIII-Ala geom							
	$\mathbf{U}_i$			$\mathbf{M}_i$			Angle
	x	y	z	x	y	z	
TOT:	2.32009×10^{1}	−5.69786	−1.72195	9.28648	−6.16513	-1.66595×10^{1}	54.43
NUC:	-7.11641×10^{-1}	1.76919	2.95169×10^{-1}	3.29490	-8.55990×10^{-2}	-5.36003×10^{-1}	114.33
EL :	2.39125×10^{1}	−7.46705	−2.01712	5.99271	−6.07956	-1.61243×10^{1}	61.15

9 Substituted Alanine: R^{μ} scalar field

As pointed out in in section 3.4, the examination of the scalar field R^{μ} can provide complementary information to the ones obtained from the R^{m} scalar field plots. In fact, in the main text we focused our attention mainly on the magnetic component of the rotatory strength, here we briefly discuss the electric component through R^{μ}. In figure 9.ESI the isosurface representations of R^{m} in the three molecules are reported. For all the systems, the major electronic contribution to electric component lies on the amide group, where the linear currents are mostly located (see figure 9 in the main text). The direct comparison of the isosurfaces extension allow to estimate the different extended to the rotatory strength contribution. In figure 10.ESI, the structures of FeII-Ala and FeIII-Ala have been superimpose along with the positive isosurfaces to be readily comparable. Subsequently, the whole picture can be retrieve combining the information from figure 9.ESI and figure 10: in the iron complexes the main contribution of the magnetic component is located on the metal whereas the electric one on the carbonyl groups.

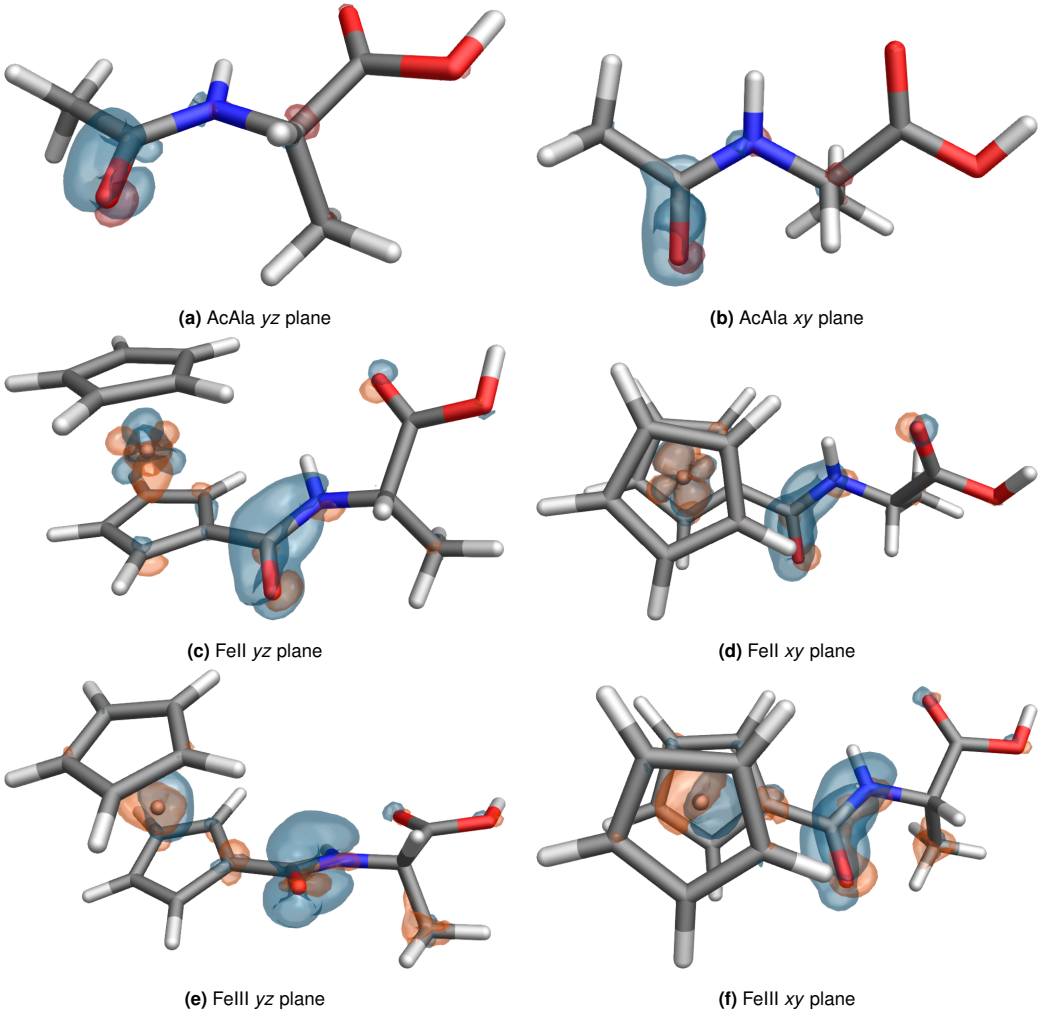

(a) AcAla *yz* plane

(b) AcAla *xy* plane

(c) FeII *yz* plane

(d) FeII *xy* plane

(e) FeIII *yz* plane

(f) FeIII *xy* plane

Fig. 9.ESI Isosurface representation of the projection of the point-by-point transition electric dipole moment on the total magnetic dipole moment (R^{μ} scalar field) for the *amide I* normal mode of AcAla (top), FeII-Ala (middle) and FeIII-Ala (bottom). Red lobes represent negative contribution to the rotatory strength, and the blue ones positive contributions. For FeII-Ala and FeIII-Ala the same isovalue has been used, whereas for AcAla, the isovalue has been reduced of one order of magnitude.

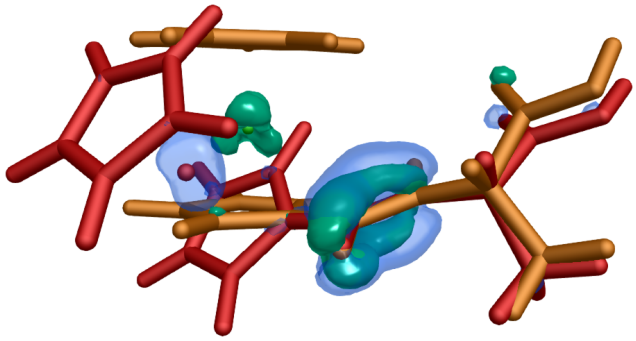

Fig. 10.ESI Positive values of the R^{μ} scalar field for the *amide I* of FeII-Ala (orange structure, green isosurface) and FeIII-Ala (red structure, transparent blue isosurface).

10 Optimized structures in XYZ format

(2*S*,3*S*)-oxirane-d_2

7

C	0.000000	0.733723	−0.374009
C	0.000000	−0.733723	−0.374009
O	0.000000	0.000000	0.856194
H	0.922216	−1.270835	−0.590362
D	−0.922216	−1.270835	−0.590362
D	0.922216	1.270835	−0.590362
H	−0.922216	1.270835	−0.590362

***S*-1,3-difluoroallene**

7

C	−0.003856	1.304108	0.343694
H	0.625133	1.915108	0.985139
C	−0.000000	0.000000	0.316450
C	0.003856	−1.304108	0.343694
H	−0.625133	−1.915108	0.985139
F	−0.807945	2.054636	−0.439708
F	0.807945	−2.054636	−0.439708

***N*-Acetyl-*L*-alanine**

18

C	−0.017951	0.012392	0.062541
O	1.211700	0.007452	0.030624
H	−1.739679	1.154849	0.272229
N	−0.733021	1.169529	0.163669
C	−0.077239	2.456569	0.302076
H	0.777620	2.343377	0.978978
C	0.438436	3.002904	−1.043544
H	0.959629	3.953740	−0.899634
H	1.134662	2.275565	−1.467562
H	−0.392781	3.151024	−1.741392
C	−1.068523	3.417265	0.930958
O	−2.253514	3.197241	1.084311
O	−0.485858	4.581345	1.286124
H	−1.181917	5.156388	1.656860
C	−0.833321	−1.264725	−0.018650
1	−0.603382	−1.769746	−0.962231
1	−0.526204	−1.930019	0.794254
1	−1.913408	−1.098164	0.042267

***N*-(ferrocene-carboxy)-(*L*)-alanine (FeII-Ala)**

34

C	−1.026337	−1.829502	3.631979
C	−2.248930	−2.569356	3.588993
C	−3.281646	−1.690184	3.137793
C	−2.699123	−0.405033	2.904268
C	−1.305646	−0.493915	3.209457
H	−0.052713	−2.222000	3.892875
H	−2.363375	−3.621229	3.814487
H	−4.314977	−1.960284	2.965296
H	−3.208826	0.474094	2.532579
H	−0.578638	0.298593	3.091284
Fe	−1.790016	−1.833339	1.706287
C	−2.207453	−1.397619	−0.261520
C	−2.556785	−2.753543	0.003366
C	−0.801900	−1.245216	0.007096
H	−2.884763	−0.626676	−0.603706
C	−1.379633	−3.440120	0.436956
H	−3.548617	−3.178189	−0.075617
C	−0.296942	−2.516009	0.432928
H	−1.330298	−4.473439	0.753185
H	0.722878	−2.701593	0.738154
C	0.000000	0.000000	0.000000
O	1.232068	0.000000	0.000000
H	−1.700093	1.119179	0.285112
N	−0.728949	1.162909	0.000000
C	−0.073148	2.439304	0.206503
H	0.843733	2.270712	0.786044
C	0.315933	3.120129	−1.118244
H	0.843242	4.060516	−0.933791
H	0.973634	2.444896	−1.671724
H	−0.574302	3.319517	−1.724483
C	−1.000598	3.309576	1.035842
O	−2.125508	3.001470	1.380998
O	−0.438355	4.493654	1.353519
H	−1.090690	4.996274	1.877661

***N*-(ferrocenium-carboxy)-(*L*)-alanine (FeIII-Ala)**

34

C	1.518438	−3.303035	2.077485
C	0.582595	−4.282249	2.543232
C	−0.342998	−3.629312	3.408237
C	0.013723	−2.252401	3.481363
C	1.162826	−2.044473	2.660357
H	2.340430	−3.474649	1.395556
H	0.563134	−5.328397	2.266960
H	−1.199395	−4.088751	3.885071
H	−0.524424	−1.487702	4.026647
H	1.647385	−1.098658	2.456474
Fe	−0.377659	−2.755824	1.426156
C	−2.019278	−1.624895	0.639948
C	−2.283142	−3.000429	0.390783
C	−0.777264	−1.288255	0.007721
H	−2.627356	−0.964418	1.245523
C	−1.215671	−3.525351	−0.391939
H	−3.121358	−3.564317	0.780155
C	−0.278912	−2.475192	−0.629563
H	−1.117472	−4.551639	−0.721231
H	0.648421	−2.539550	−1.182345
C	−0.024887	0.010656	0.031768
O	1.205684	0.011909	0.088250
H	−1.803849	1.060604	−0.069707
N	−0.791809	1.117489	−0.010438
C	−0.236828	2.465776	0.027694
H	0.547112	2.499154	0.792063
C	0.361989	2.896023	−1.323392
H	0.779229	3.903339	−1.245850
H	1.161244	2.203441	−1.598030
H	−0.404510	2.888248	−2.105215
C	−1.377538	3.382202	0.448894
O	−2.537167	3.026121	0.531169
O	−0.951788	4.627737	0.693620
H	−1.722519	5.180904	0.928181

References

1 A. C. Telea, *Data visualization: principles and practice*, AK Peters/CRC Press, 2007.

2 T. McLoughlin, R. S. Laramee, R. Peikert, F. H. Post and M. Chen, *Computer Graphics Forum*, 2010, **29**, 1807–1829.

3 J. D. Hunter, *Computing In Science & Engineering*, 2007, **9**, 90–95.

4 `http://web.mit.edu/speth/Public/streamlines.py`, Accessed: 2018-09-06.

5 J. Han, J. Pei and M. Kamber, *Data Mining: Concepts and Techniques*, Elsevier Science, 2011.

6 D. Licari, M. Fusè, A. Salvadori, M. Mendolicchio, N. Tasinato, G. Mancini and V. Barone, *Phys. Chem. Chem. Phys.*, 2018, 10.1039/C8CP03417F.

7 A. Salvadori, M. Fusè, G. Mancini, S. Rampino and V. Barone, *J. Comput. Chem.*, 2018, 10.1002/jcc.25523.

8 A. Salvadori, G. Del Frate, M. Pagliai, G. Mancini and V. Barone, *International Journal of Quantum Chemistry*, 2018, **116**, 1731–1746.

9 P. Ramachandran and G. Varoquaux, *Computing in Science Engineering*, 2011, **13**, 40–51.